Journal of Inorganic Biochemistry 114 (2012) 94–105

Contents lists available at SciVerse ScienceDirect

Journal of Inorganic Biochemistry

journal homepage: www.elsevier.com/locate/jinorgbio

Efficient DNA cleavage mediated by mononuclear mixed ligand copper(II) phenolate complexes: The role of co-ligand planarity on DNA binding and cleavage and anticancer activity

Paramasivam Jaividhya [a], Rajkumar Dhivya [b], Mohamad Abdulkadhar Akbarsha [c,d], Mallayan Palaniandavar [a,e,*]

[a] Centre for Bioinorganic Chemistry, School of Chemistry, Bharathidasan University, Tiruchirappalli 620024, Tamil Nadu, India
[b] Department of Animal Science, Bharathidasan University, Tiruchirappalli 620024, Tamil Nadu, India
[c] Mahatma Gandhi-Doerenkamp Center for Alternatives to Use of Animals in Life Science Education, Bharathidasan University, Tiruchirappalli, 620024, Tamil Nadu, India
[d] Department of Food Sciences and Nutrition, College of Food Sciences and Agriculture, King Saud University, Riyadh 11451, Saudi Arabia
[e] Central University of Tamil Nadu, Thiruvarur 610001, India

ARTICLE INFO

Article history:
Received 15 March 2012
Received in revised form 26 April 2012
Accepted 26 April 2012
Available online 8 May 2012

Keywords:
Mixed ligand copper(II) complexes
DNA binding
DNA cleavage
Anticancer activity

ABSTRACT

The new mononuclear copper(II) complexes $[Cu(L)(H_2O)_2]^+$ **1** and $[Cu(L)(diimine)]^+$ **2–6**, where LH = 2-[(2-dimethylaminoethylimino)methyl]phenol and diimine = 2,2′-bipyridine (bpy) (**2**), or 1,10-phenanthroline (phen) (**3**), or dipyrido[3,2-*f*:2′,3′-*h*]quinoxaline (dpq) (**4**) or dipyrido[3,2-*a*:2′,3′-*c*]phenazine (dppz) (**5**) or 11,12-dimethyldipyrido[3,2-*a*:2′,3′-*c*]phenazine (dmdppz) (**6**), have been isolated and characterized. The X-ray crystal structures of **2** contains the monomeric complex molecule with a trigonal bipyramidal distorted square pyramidal (TBPDSP) coordination geometry, while **4** and **6** with square pyramidal distorted trigonal bipyramidal (SPDTBP) coordination geometry. The amine nitrogen of $-NMe_2$ group of the tridentate primary ligand is located at one of the corners of the square plane in **2** and **6** but in the axial position in **4**. The interaction of the complexes with calf thymus DNA has been investigated using UV-visible and fluorescence spectroscopy, and viscosity measurements to understand the effect of diimine co-ligands on the mode and extent of DNA binding. The complexes **4** and **5** interact with calf thymus DNA more strongly than the other complexes through partial intercalation of the extended planar ring of the dpq (**4**) and dppz (**5**) co-ligands with the DNA base stack. All the complexes, except **1**, effect the double strand DNA cleavage of plasmid DNA and **5** cleaves plasmid DNA in the absence of a reductant at a concentration (40 μM) lower than **4**. It is remarkable that all the complexes display cytotoxicity against human breast cancer cell lines (MCF-7) and human cervical epidermoid carcinoma cell lines (ME 180) with potency higher than the currently used chemotherapeutic agent cisplatin and that **5** exhibits cytotoxicity higher than the other complexes.

1. Introduction

While many drug molecules are "organic" in nature, other elements in the periodic table, particularly metals, offer a much more diverse chemistry and have important therapeutic applications [1]. In modern medicine, the most striking example is cisplatin, which is a metal coordination compound containing no organic units and is currently one of the leading drugs used against cancer [2–7]. However, its effectiveness is limited by its high toxicity and incidence of drug resistance. This has provided motivation for the search for transition metal-based drugs with a wider spectrum of activity and lower systemic toxicities. Some of the recent successes are compounds based on the bis-am(m)ineplatinum(IV) and ruthenium-based coordination compounds with *N*-heterocyclic ligands, and they are presently undergoing evaluation in clinical trials [8,9]. The new compounds exploit passive and active targeting strategies to overcome aspects of drug resistance. So, it is essential to increase the variety of potential metal-based drugs, which may achieve higher activity, enabling the administration of a lower dose, attack on different types of tumor cells, overcome drug resistance problems, and exhibit better selectivity and lower toxicity than cisplatin. So, there is considerable attention focused on the design of new metal-based anticancer drugs that exhibit enhanced selectivity and novel modes of DNA interaction like non-covalent interactions that mimic the mode of interaction of biomolecules [10]. Copper [11–13] and ruthenium [14–23] complexes are regarded as promising alternatives to platinum complexes and several copper complexes [11–13,24,25] have been now proposed as potential anticancer substances, demonstrating remarkable anticancer activity and showing general toxicity lower than platinum compounds. So many other novel transition metal complexes as well as small molecule based antitumor agents have been developed and some of them are under clinical trial [26–30]. Copper(II) complexes are considered the best alternatives to cisplatin as copper is biocompatible, and exhibits a significant

* Corresponding author at: Centre for Bioinorganic Chemistry, School of Chemistry, Bharathidasan University, Tiruchirappalli 620024, Tamil Nadu, India. Tel.: +91 431 2407053; fax: +91 431 2407043.
E-mail addresses: palanim51@yahoo.com, palaniandavarm@gmail.com (M. Palaniandavar).

0162-0134/$ – see front matter © 2012 Elsevier Inc. All rights reserved.
doi:10.1016/j.jinorgbio.2012.04.018

role in biological systems. Also, synthetic copper(II) complexes have been reported to act as pharmacological agents, potential anticancer and cancer inhibiting agents [31–35]. Very recently, certain mixed ligand copper(II) complexes, which strongly bind and cleave DNA, exhibit prominent anticancer activities and regulate apoptosis [36–40]. Therefore, designing suitable copper complexes for DNA binding and cleavage under both oxidative and hydrolytic conditions, depending upon the recognition elements in the ligand, is of remarkable importance in considering the advantages of processes that produce fragments similar to those formed by restriction enzymes [41–47].

The complexes, which cleave DNA through an oxidative pathway, requires a co-reactant such as an oxidizing or reducing agent, light, or redox-active metal center in addition to the principal cleavage agent [48,49]. The disadvantage of oxidative cleavage agents is that they produce diffusible radicals which give rise to multiple cleavage sites by modifying the deoxyribose moiety, which results in fragments that cannot be re-ligated [48,49]. On the other hand, agents that promote the hydrolytic cleavage of the phosphodiester backbone of DNA do not suffer from these drawbacks [48,49]. Therefore, there has been a substantial increase in the development of reagents suitable for cleaving DNA hydrolytically under physiological conditions, which could be useful not only in molecular biology but also in drug design.

The present work stems from our continued interest in designing mixed ligand copper(II) complexes that are capable of cleaving DNA in the absence of a reductant. As part of our ongoing interest in developing new metal complexes as dsDNA binders, we have decided to explore the DNA binding properties of simple and mixed ligand complexes. So, in the present investigation we have isolated mixed ligand redox-active copper(II) complexes of the general formula $[Cu(L)(H_2O)_2](ClO_4)$ **1** and $[Cu(L)(diimine)](ClO_4)$ **2**–**6**, where LH is 2-((2-dimethylamino)ethylimino)methyl)phenol and diimine is 2,2′-bipyridine (bpy) **2** or 1,10-phenanthroline (phen) **3** or dipyrido-[3,2-*d*:2′,3′-*f*]-quinoxaline (dpq) **4** or dipyrido[3,2-d:2′,3′-f]phenazine (dppz) **5** or 11,12-dimethyldioyrido[3,2-a:2′3′-c]phenazine (dmdppz) **6** (Scheme 1). As DNA is the primary pharmacological target of many antitumor compounds, the interaction of the metal complexes **1**–**6** with calf thymus DNA (CT DNA) is of paramount importance in understanding the mechanism of tumor inhibition for the treatment of cancer. We have chosen phenolate containing ligand as primary ligand as they are considered privileged ligands in medicinal chemistry with great potential for chemotherapeutic application [50]. Also, copper(II) complexes containing phenolate ligands can show antiproliferative activities because of the properties of the coordinate ligands alone, or the structural and electronic properties which are ascribed to their coordination with metal center [50]. Very recently, we have reported mixed ligand copper(II) complexes of the type $[Cu(tdp)(tmp)](ClO_4)$, where H(tdp) is 2-[(2-(2-hydroxyethylamino)ethylimino)methyl]phenol as efficient DNA- and protein-binding and -cleaving agents, which show prominent cytotoxicity towards human cervical epidermoid carcinoma cell line (ME 180) [39]. Also, we have reported the mixed ligand copper(II) complexes of the type $[Cu(L\text{-}tyr)(diimine)](ClO_4)$, where tyr is L-tyrosine with a phenolate moiety, which act as efficient DNA binding and cleaving agents and induce apoptotic mode of cancer cell death [40]. Very recently, Reedijk and coworkers have reported that the complex [Cu(pyrimol)

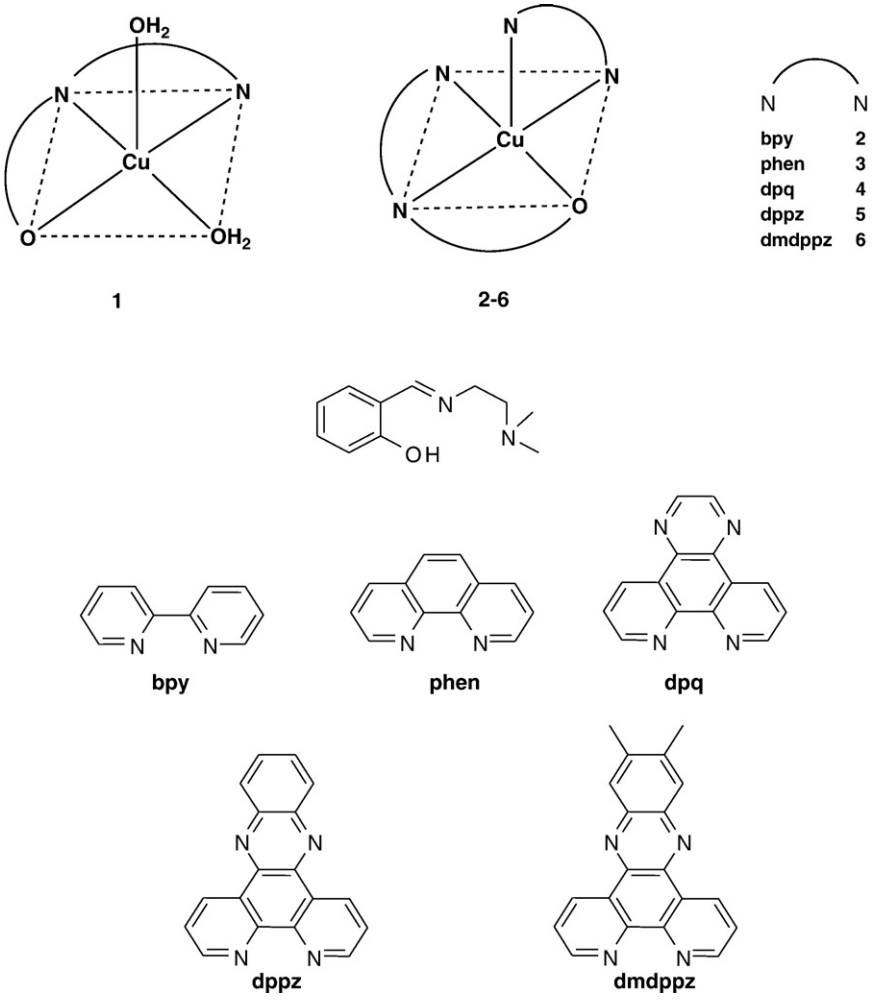

Scheme 1. Possible coordination geometries of simple and mixed ligand copper(II) complexes of primary (L) and diimine (N-N) co-ligands.

Cl], where HPyrimol is 4-methyl-2-[(pyrid-2-ylmethylene)amino]-phenol, shows efficient self-activated DNA cleavage and cytotoxic effects on L1210 murine leukemia and A2780 human ovarian carcinoma cell lines [51]. Sadler and his co-workers have reported mixed ligand bis(-salicylato)copper(II) complexes with diimines as co-ligands to exhibit cytotoxic and antiviral activities [52]. Neves et al. reported mononuclear copper(II) complexes of $[Cu(HL1)Cl_2]$, where H(L1) is 2-[(bis(pyridylmethyl)amino)methyl]-4-methyl-6-formylphenol effect double-strand DNA cleavage and amide bond cleavage [53]. The choice on the aromatic diimine co-ligand is made to find out which part of the molecule is determinant in endowing strong DNA binding affinity on the complex and also in the light of the considerations reported already by our group. The propensity and mode of DNA binding of the complexes has been studied by using absorption spectral titration, competitive DNA binding studies and viscosity measurements. The DNA cleavage properties and anticancer activities of the complexes have been also investigated. Interestingly, the complex **5**, which shows the strongest DNA binding affinity and efficient cleavage of plasmid DNA due to the partially intercalating dppz coligand, exhibits the highest anticancer activity against human breast cancer cell lines (MCF-7) and human cervical epidermoid carcinoma cell lines (ME 180) with its potency being higher than that of cisplatin.

2. Experimental

2.1. Materials

The reagents and chemicals were obtained from commercial sources (Sigma-Aldrich, USA; Himedia, India, Merck, India, Genei, Bangalore, India). Copper(II) perchlorate hexahydrate, ethidium bromide (EthBr), calf thymus (CT) DNA (highly polymerized and stored at −20 °C) (Aldrich), *N,N*-dimethylethylenediamine (Aldrich), 2,2′-bipyridine and salicylaldehyde (Loba), 1,10-phenanthrloine and 1,2-phenylenediamine (Merck) and pUC19 supercoiled DNA, agarose (Genei, Bangalore) were used as received. Ultrapure Milli Q water (18.2 mΩ) was used in all experiments. Tris–HCl was prepared by the reported procedure [54]. The commercial solvents were distilled and then used for preparation of complexes.

2.2. Experimental methods

Microanalyses (C, H and N) were carried out with a Vario EL elemental analyzer. UV–VIS spectroscopy was recorded on a Shimadzu 2450 UV-VIS spectrophotometer using cuvettes of 1 cm path length. ^{1}H NMR spectra were recorded on a Bruker 400 MHz NMR spectrometer. Mass spectrometry was performed on QTOF ESI-MS spectrometer. Emission intensity measurements were carried out by using a Jasco F 6500 spectrofluorometer. The viscosity measurements were carried out on a Schott Gerate AVS 310 automated viscometer thermostat at 25 °C in a constant temperature bath.

Solutions of DNA in the buffer 50 mM NaCl/5 mM Tris–HCl buffer (pH = 7.1) in water gave the ratio of UV absorbance at 260 and 280 nm, A_{260}/A_{280}, of 1.9, indicating that the DNA was sufficiently free of protein [55]. Concentrated stock solutions of DNA were prepared in a 50 mM NaCl/5 mM Tris–HCl buffer and sonicated for 25 cycles, where each cycle consisted of 30 s with 1 min intervals using Branson Ultra Probe sonicator. The concentration of CT DNA in nucleotide phosphate (NP) was determined by UV absorbance at 260 nm after 1:100 dilutions by taking the extinction coefficient, ε_{260} as 6600 M^{-1} cm^{-1}. Stock solutions of DNA were stored at 4 °C and used after no more than 4 days. Supercoiled plasmid pUC19 DNA was stored at: −20 °C and the concentration of pUC19 DNA in base pairs were determined by UV absorbance at 260 nm after appropriate dilutions taking ε_{260} as 13100 M^{-1} cm^{-1} [39]. Concentrated stock solutions of metal complexes were prepared by dissolving calculated amounts of copper complexes in respective amounts of solvent and diluted suitably with the corresponding buffer to required concentrations for all experiments. The ability of **1**–**6** to cleave DNA was examined by following the conversion of supercoiled plasmid DNA to open circular DNA or linear DNA using agarose gel electrophoresis to separate the cleavage products.

2.3. Synthesis of ligands

2.3.1. Synthesis of 2-((2-dimethylamino)ethyliminomethyl)phenol

Salicylaldehyde (1.02 g, 10 mmol) in methanol (20 mL) was added dropwise to *N,N′*-di-methylethylenediamine (0.88 g, 10 mmol) in methanol (10 mL). The mixture was stirred for 24 h to get a bright yellow solution. The resulting solution was evaporated, the yellow oily residue dried in vacuum and used as such for preparing the copper(II) complexes (yield, 1.83 g, 95%). ^{1}H NMR ($CDCl_3$, 400 MHz): (OH, J = 5.0, 1.0, 1H, HPy); 8.57 (s, 1H, HC = N); 8.33 (dt, J = 7.8, 1.0, 1H, HPy); 7.81 (tq, J = 7.8, 1.8, 1H, HPy); 7.38–7.35 (m, 1H, HPy); 7.28–7.16 (m, 3H, HPh); 7.08 (dd, J = 7.8, 1.3, 1H, HPh); 2.47 (3H, H_3C).

2.3.2. Synthesis of diimine ligands

The diimine ligands dpq [56], dppz [57], and 11,12-dmdppz [57] were synthesized according to literature protocols.

Caution! During handling of perchlorate salts of metal complexes with organic ligands care should be taken because of the possibility of explosion.

2.4. Preparation of copper(II) complexes

2.4.1. Preparation of $[Cu(L)(H_2O)_2](ClO_4)$ (1)

The copper(II) complex was isolated by adding 2-((2-dimethylamino) ethyl-iminomethyl)phenol (0.10 g, 0.5 mmol), which was deprotonated by treating with triethylamine (0.5 mmol) in methanol solution, to copper(II) perchlorate (0.19 g, 0.5 mmol) in methanol (10 mL) and then stirring the solution at 40 °C for 1 h. The resulting precipitate was collected by suction filtration, washed with cold methanol and finally dried in vacuum over P_4O_{10}. Anal. Calcd. for $[Cu(L)(H_2O)](ClO_4)$: C, 45.23; H, 6.52; N, 9.52. Found: C, 45.43 45.23; H, 6.58; N, 9.63%. Yield: 0.15 g (60%).

2.4.2. Preparation of $[Cu(L)(bpy)](ClO_4)$ (2)

The complex **2** was prepared by addition of a methanolic solution (10 mL) of bpy (0.078 g, 0.5 mmol) and 2-((2-dimethylamino) ethyliminomethyl)phenol (0.10 g, 0.5 mmol), which was deprotonated by using triethylamine (0.5 mmol), to a solution of copper(II) perchlorate hexahydrate (0.185 g, 0.5 mmol) in methanol (10 mL) and then stirring at 40 °C for 2 h. The green crystalline solid obtained was collected by suction filtration, washed with small amounts of cold methanol and diethyl ether and then dried in vacuum. Green colored crystals of **2** suitable for X-ray diffraction studies were obtained by dissolving the complex in aqueous methanol and allowing it to crystallize. Anal. Calcd. for $[Cu(L)(bpy)](ClO_4)$: C, 49.23; H, 4.22; N, 10.52. Found: C, 49.41; H, 4.54; N, 10.98%. Yield: 0.21 g (80%).

2.4.3. Preparation of $[Cu(L)(phen)](ClO_4)$ (3)

This complex was prepared by adopting the procedure used for the isolation of **2** but using phen instead of bpy. The dark green crystalline solid obtained was collected by suction filtration, washed with small amounts of cold methanol and diethyl ether and then dried in vacuum. Anal. Calcd for $[Cu(L)(phen)](ClO_4)$: C, 51.34; H, 4.34; N, 10.48. Found: C, 51.69 (51.34); H, 4.56; N, 10.52%. Yield: 0.24 g (90%).

2.4.4. Preparation of $[Cu(L)(dpq)](ClO_4)$ (4)

This complex was prepared by adopting the procedure used for the isolation of **2** but using dpq instead of bpy. Dark green colored crystals of **4** suitable for X-ray diffraction studies were obtained by dissolving the complex in aqueous methanol and allowing it to crystallize. Anal. Calcd for $[Cu(L)(dpq)](ClO_4)$: C, 51.20; H. 3.62; N, 14.33. Found: 51.49; H, 3.95 N, 14.35%. Yield: 0.22 g (76%).

2.4.5. Preparation of [Cu(L)(dppz)](ClO4) (5)

This complex was prepared by adopting the procedure used for the isolation of **2** but using dppz instead of bpy. The green crystalline solid obtained was collected by suction filtration, washed with small amounts of cold methanol and diethyl ether and then dried in vacuum. Anal. Calcd. for [Cu(L)(dppz)](ClO4): C, 54.10; H, 3.60; N, 13.20. Found: C, 54.72; H, 3.96; N, 13.33%. Electrospray ionization mass spectrometry (ESI-MS): $[Cu(L)(dppz)]^+$ displays a peak at *m/z* 536.18 (calcd. 536.14). Yield: 0.25 g (80%).

2.4.6. Preparation of [Cu(L)(dmdppz)](ClO4) (6)

This complex was prepared by adopting the procedure used for the isolation of **2** but using 11,12-dmdppz instead of bpy. The green crystalline solid obtained was collected by suction filtration, washed with small amounts of cold methanol and diethyl ether and then dried in vacuum. Green colored crystals of **6** suitable for X-ray diffraction studies were obtained by dissolving the complex in aqueous methanol and allowing it for crystallization. Anal. Calcd. for [Cu(L)(dmdppz)](ClO4): C, 56.02, H, 4.60, N, 12.33. Found: C, 56.10; H, 4.60, N, 12.65%. Yield: 0.24 g (72%).

2.5. X-ray crystallography

The single crystals of **2**, **4** and **6** of suitable size selected from the mother liquor were mounted on the tip of a glass fiber and cemented using epoxy resin. Intensity data for the crystals were collected using MoKα (λ = 0.71073 Å) radiation on a Bruker SMART APEX diffractometer equipped with a CCD area detector at 100 and 293 K. The SMART [58] program was used for collecting frames of data, indexing reflections, and determination of lattice parameters; SAINT program for integration of the intensity of reflections and scaling; SADABS [59] program for absorption correction, and the SHELXTL [60] program for space group and structure determination, and least-squares refinements on F^2. The structure was solved by heavy atom method and other non-hydrogen atoms were located in successive difference Fourier syntheses. Crystal data and additional details of the data collection and refinement of the structure are presented in Table 1. The selected bond lengths and angles are listed in Table 2.

2.6. DNA binding experiments

2.6.1. Electronic absorption and fluorescence spectra

Concentrated stock solutions of metal complexes were prepared by dissolving them in aqueous methanol (1:5, methanol/water) and diluting them with 50 mM NaCl/5 mM Tris–HCl buffer solution at pH 7.1 buffer to required concentrations for all the experiments. For absorption and emission spectral experiments the DNA solutions were pretreated with solutions of metal complexes to ensure no change in the metal complex concentrations. Absorption spectral titration experiments were performed by maintaining a constant concentration of the complex and varying the nucleic acid concentration. This was achieved by dissolving an appropriate amount of the metal complex and DNA stock solutions while maintaining the total volume constant (1 mL). This results in a series of solutions with varying concentrations of DNA but with a constant concentration of the complex. The absorbance (A) was recorded after successive additions of CT DNA.

The EthBr displacement assay was used to determine the apparent DNA binding constants (K_{app}) of the complexes. The emission intensity of EthBr was used as spectral probe, as it is known to show reduced emission intensity in buffer solution because of solvent quenching, and an enhancement in emission intensity is observed when EthBr intercalatively binds to CT DNA [61]. The competitive binding of complexes **1**–**6** to CT DNA could lead to the displacement of the EthBr, exposing it for solvent quenching of the emission. The binding ability of the complexes to DNA was determined from the extent of reduction of the EthBr emission intensity.

Table 1
Crystallographic data for **2**, **4** and **6.**

	[Cu(L)(bpy)]ClO4 (2)	[Cu(L)(dpq)]ClO4 (4)	[Cu(L)(dmdppz)]ClO4 (6)
Empirical formula	C21 H23 Cl Cu N4 O5	C25 H23 Cl Cu N6 O7	C62 H57 Cl2 Cu2 N12 O10
Formula weight	510.42	618.48	1328.18
Crystal system	Triclinic	Monoclinic	Triclinic
Space group	P-1	P2(1)/c	P-1
Crystal size	0.20 × 0.20 × 0.22	0.12 × 0.10 × 0.08	0.20 × 0.20 × 0.22
Temperature (K)	293	293	293
λ, Å (Mo K_α)	1.158	0.977	0.812
a, Å	7.430 (2)	8.24400(6)	13.4467(7)
b, Å	12.212 (3)	17.3817(5)	15.0111(7)
c, Å	12.693 (3)	18.7260(6)	16.2537(8)
α °	88.72 (2)	90.00	88.429(4)
β°	73.13 (3)	97.197 (3)	82.144(3)
γ°	84.52 (2)	90.00	80.612(3)
Z	2	4	2
Density (calculated), Mg/m^3	1.545	1.543	1.376
θ for data collection	1.68, 34.12	1.60, 29.61	1.37, 22.33
Refinement method	Full-matrix least-squares on F^2	Full-matrix least-squares on F^2	Full-matrix least-squares on F^2
Unique reflections [$R_{(int)}$]	26976/7588 [R (int) = 0.028]	31029/7462 [R (int) = 0.0306]	43435/8113 [R (int) = 0.1146]
F (000)	526	1268	1370
[a]R indices (all data)	R = 0.0518, wR2 = 0.1537	R = 0.0520, wR2 = 0.1527	R = 0.0806, wR2 = 0.2126
S	1.051	1.077	0.997
Largest difference in peak and hole, e $Å^{-3}$	1.052, −0.756	0.548, −0.772	1.105, −0.384

[a] $R = \Sigma \mid\mid F_o \mid - \mid F_c \mid\mid / \Sigma \mid F_o \mid$, [b] $wR_2 = \{\Sigma\, w[(F_o^2 - F_c^2)^2 / \Sigma\, w\,[(F_o^2)^2]\}^{1/2}$.

Table 2
Selected bond distances (Å) and angles (degree) for complexes **2**, **4** and **6.**

Complex 2			
Cu1 – O5	1.917(18)	O5 – Cu1 – N1	93.29(9)
Cu1 – N1	1.932 (2)	O5 – Cu1 – N2	165.27(9)
Cu1 – N2	2.085 (2)	O5 – Cu1 – N3	99.07(9)
Cu1 – N3	2.238 (2)	O5 – Cu1 – N4	88.08(8)
Cu1 – N4	2.024 (2)	N1 – Cu1 – N2	83.95(9)
		N1 – Cu1 – N3	108.78(9)
		N1 – Cu1 – N4	173.52(8)
		N2 – Cu1 – N3	95.52(9)
		N2 – Cu1 – N4	93.12(9)
		N3 – Cu1 – N4	77.21(9)
Complex 4			
Cu1 – N1	1.937(3)	O1 – Cu1 – N1	91.77(10)
Cu1 – N2	2.092(3)	O1 – Cu1 – N4	89.90 (9)
Cu1 – N3	2.247(3)	N1 – Cu1 – N4	178.09 (10)
Cu1 – N4	2.026(2)	O1 – Cu1 – N2	155.82 (11)
Cu1 – O1	1.928(1)	N1 – Cu1 – N2	83.87 (12)
		N4 – Cu1 – N2	94.98 (11)
		O1 – Cu1 – N3	107.21 (10)
		N1 – Cu1 – N3	100.92 (11)
		N4 – Cu1 – N3	77.69 (9)
		N2 – Cu1 – N3	96.96 (10)
Complex 6			
Cu1-O1	1.918 (6)	O1 – Cu1 – N1	93.7(3)
Cu1-N1	1.925 (8)	O1 – Cu1 – N2	153.6(3)
Cu1-N2	2.081(8)	O1 – Cu1 – N3	104.4(3)
Cu1-N3	2.231 (8)	O1 – Cu1 – N4	89.2(3)
Cu1-N4	2.025 (7)	N1 – Cu1 – N3	100.2(3)
		N1 – Cu1 – N4	177.0(3)
		N1 – Cu1 – N2	83.3(4)
		N2 – Cu1 – N4	94.6(3)
		N3 – Cu1 – N4	78.2(3)
		N2 – Cu1 – N3	101.9(3)

2.6.2. Viscosity measurements

For viscosity measurements, CT DNA concentration was kept constant (500 μM in NP) and the concentration of metal complexes varied ($1/R = [Cu]/[DNA] = 0.0–0.50$). The flow times were noted from the digital timer attached to the viscometer. Data are presented as η/η_0 vs. $1/R$, where η is the relative viscosity of DNA in the presence of the copper(II) complex and η_0 is the relative viscosity of DNA alone. Relative viscosity values were calculated from the observed flow time of the DNA solution (t) corrected for the flow time of the buffer alone (t_0), using the expression $\eta_0 = (t - t_0)/t_0$.

2.7. DNA cleavage experiments

The interaction of complexes with supercoiled pUC19 DNA was monitored using agarose gel electrophoresis. In reactions using supercoiled pUC19 DNA plasmid DNA (SC form, 40 μM) in a 50 mM NaCl/5 mM Tris–HCl buffer solution at pH 7.1 was treated with metal complexes in the same buffer. In each experiment supercoiled pUC19 DNA (SC form, 40 μM) was treated with different concentrations of metal complexes and was monitored using agarose gel electrophoresis. The samples were then incubated for 1 h for 37 °C and analyzed for the cleaved products using gel electrophoresis as discussed below. A loading buffer containing 22% bromophenol blue, 0.22% xylene cyanol and 30% glycerol (3 μL) was added and electrophoresis performed at 60 V for 5 h in Tris–Acetate–EDTA (TAE) buffer (40 mM Tris base, 20 mM acetic acid, 1 mM EDTA) using 1% agarose gel containing 1.0 μg mL^{-1} ethidium bromide. The gels were viewed in a Gel doc system and photographed using a CCD camera (Alpha Innotech Corporation). The intensities of supercoiled DNA were corrected by a factor of 1.47 as a result of its lower staining capacity by ethidium bromide [62]. The cleavage efficiency was measured by determining the ability of the complex to convert the supercoiled DNA (SC, form I) to nicked circular form (NC) and linear form (LC). For mechanistic investigations, experiments were carried out in the presence of radical scavenging agents, viz., DMSO (6 μL), methanol (10 μL) and glycerol (5 μL), which were added to SC DNA prior to the addition of the complex. For kinetic measurements, DNA cleavage rates at various complex concentrations were measured in a TAE buffer (pH 8.0) at 37 °C for different intervals of time. The decrease in the intensities of form I were then plotted against complex concentrations, and these were fitted well with a single-exponential decay curve (pseudo-first-order kinetics) by use of Eq. (1), where y_0 is the initial percentage of a form of DNA, y is the specific form of DNA at time t, constant is the percentage of uncleaved DNA, K_{obs} is the hydrolysis rate or apparent rate constant, and V_{max} is the maximal reaction velocity [63]. Careful optimization of electrophoretic and densitometric techniques led to pseudo-first-order kinetics and allowed the determination of true Michaelis–Menten kinetic parameters.

$$y = (y_0 - \text{constant})\exp(-K_{obs}x) + \text{constant} \quad (1)$$

K_{obs} versus [Cu] was plotted and fit using Eq. (2), which allows the determination of both the rate constants and Michaelis–Menten-"type" kinetic values.

$$K_{obs} = V_{max}[\text{catalyst}]/(K_M + [\text{catalyst}]) \quad (2)$$

2.8. 3-(4,5-dimethylthiazol-2-yl)-2,5-diphenyltetrazolium bromide (MTT) Assay

MTT assay was carried out as described previously [64]. The complexes in the concentration range of 0.05–50 μg/mL, dissolved in DMSO (Sigma-Aldrich, St. Louis, MO, USA) were added to the wells 24 h after seeding of 5×10^3 cells per well in 200 μL of fresh culture medium. DMSO was used as the vehicle control. After 24 and 48 h, 20 μL of MTT solution [5 mg/mL in phosphate-buffered saline (PBS)] was added to each well and the plates were wrapped with aluminum foil and incubated for 4 h at 37 °C. The purple formazan product formed was dissolved by addition of 100 μL of 100% DMSO to each well. The absorbance was monitored at 570 nm (measurement) and 630 nm (reference) using a 96 well plate reader (Bio-Rad, Hercules, CA, USA). The stock solutions of the metal complexes were prepared in DMSO and in all the experiments the percentage of DMSO was maintained in the range of 0.1–1%. DMSO by itself was found to be non-toxic to the cells till 1% concentration. Data were collected for four replicates each and used to calculate the mean. The percentage inhibition was calculated from this data using the formula:

$$= \frac{\text{Mean OD of untreated cells(control)} - \text{Mean OD of treated cells}}{\text{Mean OD of untreated cells(control)}} \times 100$$

The IC_{50} values were calculated using *Table Curve 2D*, version 5.01.

2.8. AO/EB staining assay

For both suspension and adherent cells, 96-well plates were centrifuged at 1000 RPM (129 *g*) for 5 min using a Beckman Model TJ-6 centrifuge with inserts for 96-well plates. Acridine orange/ethidium bromide (AO/EB) dye mix (8 mL) was added to each well, and cells were viewed under the fluorescent microscope (Carl Zeiss, Jena, Germany) fitted with a 377 - 355 nm filter, and observed at ×400 magnification. Tests were done in triplicate, counting a minimum of 100 total cells each.

3. Results and discussion

3.1. Synthesis and solution properties of copper(II) complexes

The Schiff base ligand 2-((2-dimethylamino)ethylimino)methyl) phenol was synthesized by condensing *N,N′*-dimethylethylenediamine with salicylaldehyde in methanol solution. The ligand was characterized by ^{1}H NMR spectra. The complex **1** was prepared by treating copper(II) perchlorate hexahydrate with the Schiff base ligand in equimolar quantities in methanol as solvent. The mixed ligand copper(II) complexes **2**–**6** were prepared by treating copper(II) perchlorate hexahydrate with the Schiff base ligand and the corresponding diimine in equimolar quantities using methanol as solvent. The complexes have been isolated as a green colored powders. Based on elemental analysis the complexes were formulated as $[Cu(L)(H_2O)_2](ClO_4)$ **1** and $[Cu(L)(diimine)](ClO_4)$ **2–6,** and the stoichiometries of **2, 4** and **6** were confirmed by single crystal X-ray structure determination. The complexes are moderately soluble in common organic solvents such as MeCN and MeOH/H_2O, less soluble in water and insoluble in hydrocarbon solvents. They are stable in the solid state as well as in the solution phase. The electronic absorption spectra of all the six complexes in methanol:water (1:4 v/v) solution are very similar to each other and show a broad low energy ligand field (LF) band in the visible region 615–650 nm (Table 3). The intense absorption band observed in the UV region (235–275 nm) is attributed to the intraligand $\pi \rightarrow \pi^*$ transition in the coordinated diimines. The low intensity band (350–385 nm), which is assignable to phenolate anion to Cu(II) ligand to metal charge transfer (LMCT) transition, reveals the involvement of the phenolate oxygen atom in coordination even in solution. In order to probe the solution stability of the complexes, we have performed UV–VIS spectral measurements for 5 mM solution of all the complexes at room temperature at various time intervals. The LF band in the visible region (615–650 nm) of all the complexes remained unaffected over a period of at least 7 days revealing that the complexes are stable in solution at room temperature.

Table 3
Electronic spectral[a] properties of copper(II) complexes.

Complex	λ_{max} in nm (ε, M^{-1} cm^{-1})		
	Ligand field[b]	Ligand based[c]	CT transition
$[Cu(L)(H_2O)_2](ClO_4)$ **1**	618 (232)	235 (43256)	356 (5324)
$[Cu(L)(bpy)](ClO_4)$ **2**	644 (140)	272 (25810)	372 (4856)
$[Cu(L)(phen)](ClO_4)$ **3**	638 (128)	269 (51689)	370 (4129)
$[Cu(L)(dpq)](ClO_4)$ **4**	628 (165)	253 (89837)	372 (5294)
$[Cu(L)(dppz)](ClO_4)$ **5**	630 (219)	270 (108124)	375 (19856)
$[Cu(L)(dmdppz)](ClO_4)$ **6**	633 (168)	275 (100918)	384 (26331)

[a] In methanol solution.
[b] Concentration 5×10^{-3} M.
[c] Concentration 1×10^{-5} M.

3.2. Description of crystal structures of $[Cu(L)(bpy)](ClO_4)$ 2, $[Cu(L)(dpq)](ClO_4)$ 4 and $[Cu(L)(dmdppz)](ClO_4)$ 6

3.2.1. Description of the structure of $[Cu(L)(bpy)](ClO_4)$ 2

The crystal structure of $[Cu(L)(bpy)](ClO_4)$ **2** consists of monomeric units of the complex cation. An ORTEP view of the coordination environment around copper(II) in the complex cation is shown in Fig. 1 and the selected bond distances and angles are listed in Table 2. The copper is coordinated by one phenolate oxygen and two nitrogen atoms from the Schiff base ligand and two nitrogen atoms from bpy co-ligand. The coordination geometry around copper(II) is described as trigonal bipyramidal distorted square pyramidal (TBPDSP) as evident from the value of the trigonal index τ, 0.14 [$\tau = (\alpha-\beta)/60$, where $\alpha = 173.52°$ and $\beta = 165.27°$; τ is 1 for a perfect trigonal bipyramidal geometry and is zero for a perfect square pyramidal geometry] [65]. The phenolate oxygen O5 and N1 and N2 nitrogen atoms of the deprotonated primary ligand and N4 nitrogen atom of bpy occupy the four corners of the square plane and the N3 nitrogen atom of the bpy co-ligand occupies the axial position. The Cu-$O_{phenolate}$ bond distance (1.917(18)–1.927(2) Å) is in the range expected for copper(II) phenolate complexes [39]. The Cu – N2 bond distance (2.085(2) Å) is longer than the Cu-$N1_{imine}$ bond distance (1.932(2) Å), which is expected of the sp^3 and sp^2 hybridizations, respectively, of the amine and imine nitrogen atoms. Also, the presence of methyl groups on the N2 amine nitrogen renders the nitrogen lone pair orbital not exactly oriented along the $d_x2_{-y}2$ orbital of copper(II) making the Cu – $N2_{amine}$ bond longer than the Cu – $N1_{amine}$ bond [66–68]. The axial Cu – N3 bond (2.238(2) Å) is longer than all the bonds (1.932–2.085 Å) in the equatorial plane, which is due to the presence of two electrons in the d_z2 orbital of copper(II).

3.2.2. Description of the structure of $[Cu(L)(dpq)](ClO_4)$ 4

The crystal structure of $[Cu(L)(dpq)](ClO_4)$ **4** consists of discrete molecules of the complex cation $[Cu(L)(dpq)]^+$. The ORTEP view of the cation is given in Fig. 2 and the selected bond distances and angles are listed in Table 2. The value (0.37) of the trigonality index τ reveals that the coordination geometry around copper(II) is best described as square pyramidal distorted trigonal bipyramidal (SPDTBP). In this geometry, two of the corners of the square plane are occupied by the phenolate oxygen atom O1 and the imine nitrogen atom N1 of the primary ligand and the remaining two corners by the N3 and N4 nitrogen atoms of dpq co-ligand and the axial position occupied by N2 amine nitrogen atom of the primary ligand. The Cu – N (Cu – $N4_{imine}$, 2.026(2), Cu – N3, 2.247(3); Cu – $N1_{dpq}$, 1.937(3); Cu – $N2_{dpq}$, 2.092(3) Å) and the Cu – O1 (1.928(1) Å) bond lengths are similar to those in **2**. Thus the axial Cu – N3 bond (2.247(3) Å) is longer than all the bonds (1.928–2.092 Å) in the equatorial plane, which is due to the presence of two electrons in the d_z2 orbital of copper(II). The improper orientation of the lone pair on N2 nitrogen of $-NMe_2$ group towards the $d_x2_{-y}2$ orbital also would contribute to the longer Cu – N2 bond distance. Interestingly, the coordination geometry of **4** differs from that of **2** in that the tridentate Schiff base ligand is meridionally coordinated in **2** but in an equatorial-axial mode in **4**. Upon replacing bpy in **2** by the strongly coordinating dpq co-ligand (Cu – N1, 1.937(3); Cu – N2, 2.092(3) Å) in the equatorial x–y plane, the sterically hindered N2 amine nitrogen strongly coordinated in **2** defaults to a more weakly bound z-axial position in **4**.

3.2.3. Description of the structure of $[Cu(L)(dmdppz)](ClO_4)$ 6

An ORTEP drawing of the complex cation of $[Cu(L)(dmdppz)](ClO_4)$ **6** is shown in Fig. 3 and selected bond distances and angles are listed in Table 2. The Cu(II) in each cation is coordinated by the phenolate oxygen atom (O1) and two nitrogen atoms (N1, N2) of the Schiff base ligand and two nitrogen (N3, N4) atoms of the dmdppz co-ligand. The value (0.39) of the trigonality index τ of **6** reveals that the coordination geometry around copper(II) is best described as square pyramidal distorted trigonal bipyramidal (SPDTBP) [65]. The two amine nitrogen atoms (N1, N2) and the phenolate oxygen atom (O1) of the meridionally coordinated Schiff base ligand and one of the imine nitrogen atoms (N4) of dmdppz occupy the corners of the CuN_3O square plane of this geometry. The axial position is occupied by the other nitrogen atom (N3) of the dmdppz at a distance of 2.231 Å, longer than the equatorial

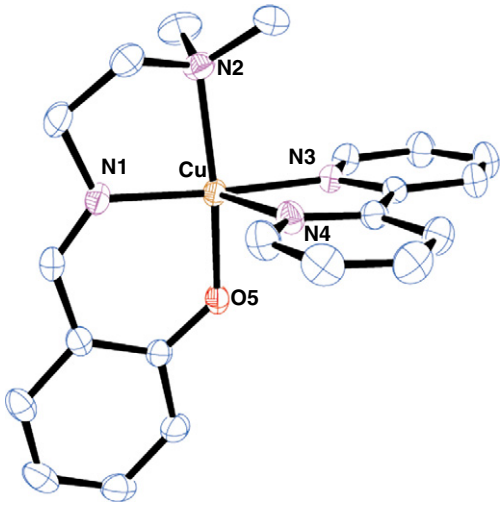

Fig. 1. ORTEP representation of $[Cu(L)(bpy)]^+$ **2** showing the atom numbering scheme and the thermal motion ellipsoids (50% probability level) for the non-hydrogen atoms. Hydrogen atoms and perchlorate counter ion are omitted for clarity.

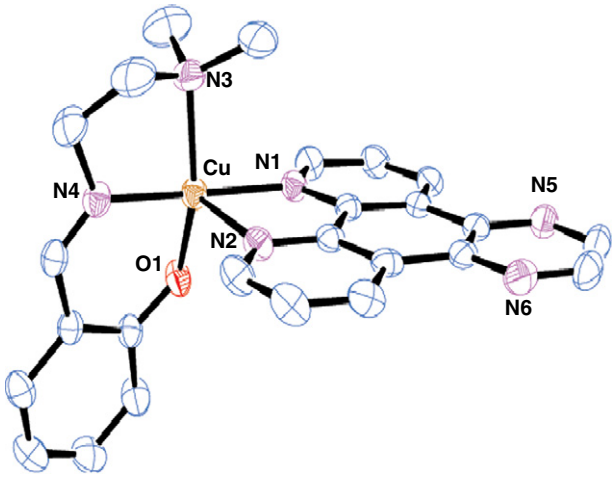

Fig. 2. ORTEP representation of $[Cu(L)(dpq)]^+$ **4** showing the atom numbering scheme and the thermal motion ellipsoids (50% probability level) for the non-hydrogen atoms. Hydrogen atoms and perchlorate counter ion, water molecules are omitted for clarity.

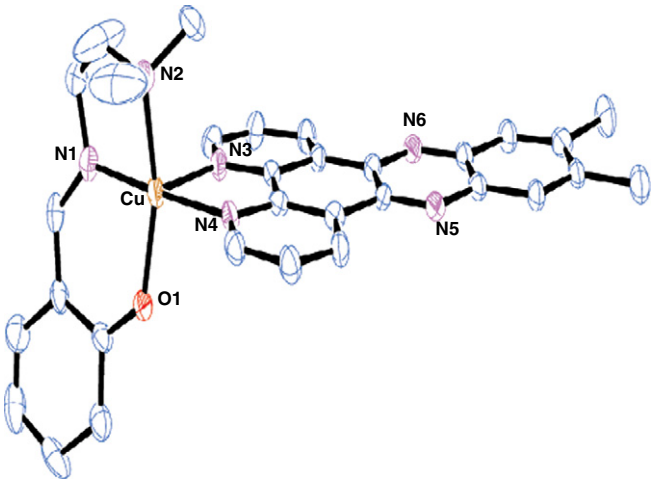

Fig. 3. ORTEP representation of $[Cu(L)(dmdppz)]^+$ **6** showing the atom numbering scheme and the thermal motion ellipsoids (50% probability level) for the non-hydrogen atoms. Hydrogen atoms and perchlorate counter ion are omitted for clarity.

atoms (Cu-O1, 1.918(6) Å; Cu-N1, 1.925(8) Å; Cu-N2, 2.081(8) Å; Cu-N4, 2.025(7) Å) as a consequence of the presence of two electrons in d_z^2 orbital of copper(II). The Cu – $N2_{amine}$ bond (Cu – N2, 2.081(8) Å) is longer than the Cu – N_{imine} bond (Cu – N1, 1.925(8) Å) formed by the primary ligand, which is expected of sp^3 and sp^2 hybridizations of the amine (N2) and imine (N1) nitrogen atoms respectively. The coordination geometry of **6** is similar to that of **2**; however, the higher trigonality index of **6** is due to the stronger coordination of dmdppz and the steric clash of the sterically hindered $-NMe_2$ group with the dmdppz.

3.3. DNA binding studies

3.3.1. Absorption spectral titration

Electronic absorption spectroscopy is an effective method of examining the mode and extent of binding of a metal complex with DNA. Upon adding CT DNA to **1–6** (R = [DNA]/[complex] = 1– 25) in 5 mM Tris–HCl/50 mM NaCl buffer solution, the ligand-based $\pi \rightarrow \pi^*$ spectral band exhibits hypochromism (20–82%) with or without red-shifts in band position. Typical absorption spectral traces of **5** with increasing concentration of CT DNA are shown in Fig. 4. As the extent of hypochromism is commonly associated with the strength of DNA interaction, the observed order of decrease in hypochromism (Table 4), **6**<**5**>**4**>**3**>**2**>**1**, reflects the decreasing DNA binding affinities of the complexes in this order (cf. below). All the complexes, except **1,** can partially insert their diimine co-ligands into the DNA base pairs, and if the coupling π orbital of diimine is partially filled with electrons, it results in a decrease in the transition probabilities and concomitantly in hypochromism [69]. In order to compare the DNA binding affinities quantitatively, the intrinsic binding constants K_b of **1–6** bound to CT DNA were obtained by monitoring the changes in absorbance of the $\pi \rightarrow \pi^*$ spectral band (253–275 nm) with increasing concentration of DNA by using the following equation [70],

$$[DNA]/(\varepsilon_a - \varepsilon_f) = [DNA]/(\varepsilon_b - \varepsilon_f) + 1/K_b(\varepsilon_b - \varepsilon_f)$$

where [DNA] is the concentration of DNA in base pairs, the apparent absorption coefficient ε_a, ε_f and ε_b corresponds to A_{obs}/[Complex], the extinction coefficient for the free copper complex and the extinction coefficient for the free copper complex in the fully bound form, respectively. In the plot of [DNA]/(ε_a–ε_f) versus [DNA], the value of K_b is given by the ratio of slope to intercept. The binding constants determined (K_b, 1.3×10^2–1.0×10^5 M^{-1}) varies in the order: **6**<**5**>**4**>**3**>**2**>**1**, which is the same as that for the hypochromism (cf. above). They are lower than those observed [71] for the typical classical intercalator

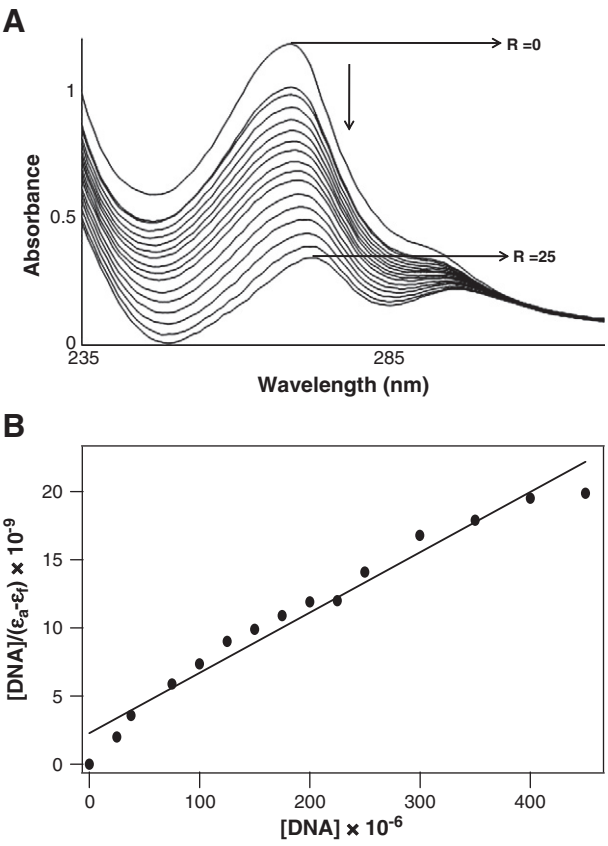

Fig. 4. (A) Absorption spectra of $[Cu(L)(dppz)](ClO_4)$ **5** (1×10^{-5} M) in 5 mM Tris–HCl/50 mM NaCl buffer at pH 7.1 in the absence (R = [DNA]/[complex] = 0) and presence of (R = 1–25) increasing amounts of DNA. (B) Plot of [DNA]/(ε_a–ε_f) vs [DNA] for $[Cu(L)(dppz)](ClO_4)$ **5**.

ethidium bromide (EthBr) (K_b, 4.94×10^5 M^{-1} in 25 mM Tris–HCl/40 mM NaCl buffer, pH 7.9) and the partially intercalating Ru(II) complex cations [72] $[Ru(bpy)_2(dpq)]^{2+}$ (K_b, 1.4×10^6 M^{-1} in 25 mM Tris–HCl/40 mM NaCl buffer, pH 7.9) and $[Ru(bpy)_2(dppz)]^{2+}$ (K_b, 1.35×10^6 M^{-1} in 25 mM Tris–HCl/40 mM NaCl buffer, pH 7.1), both bound to CT DNA. The higher red-shifts (4–9 nm) observed for **3**, **4** and **5** suggest that the coordinated phen, dpq and dppz rings respectively in them are inserted into the DNA base pairs leading to the partial intercalative interaction of the complexes with DNA. The observed K_b value of **5** is higher than that of **4** (Fig. 4B), which is supported by the higher red-shift observed for the former (9 nm). The π stacking of the extended aromatic dppz ring in **5** into the DNA base pairs (Fig. 4A) is deeper than that of dpq ring in **4**. In turn, the coordinated dpq ring in **4** with a larger aromatic ring surface area is engaged in partial insertion in between the base pairs of DNA much deeper than the coordinated phen ring in **3**, leading to the higher DNA binding affinity of **4**. This is consistent with the higher hypochromism (cf. above) and the higher red-shift observed for **4** (**4**, 5; **3**, 4 nm). Thus, in general, a planar extension of the intercalating ligand would increase the strength of interaction of the complexes with DNA. The complex **6** also exhibits hypochromism but with a red-shift (3 nm) smaller than the phen complex **2**. This is expected as the incorporation of methyl groups on dppz ligand would hinder the insertion of the dppz ring in between the DNA base pairs [73]. The complex **2** with two non-planar pyridine rings is obviously involved in electrostatic binding to DNA via the exterior of phosphate esters. Thus, the number of aromatic rings in the diimine co-ligand and substitution on the dppz ring dictate the DNA binding affinity and binding structure of the mixed ligand complexes. Also, the mixed ligand copper(II) complexes $[Cu(tdp)(diimine)]^+$ (K_b, $0.7–9.0\times10^5$ M^{-1}) [39] exhibit higher order of binding affinities than

Table 4
Ligand based absorption and emission spectral properties of Cu(II) complexes bound[a] to calf thymus DNA.

Complex			Ligand based				
	λ_{max} (nm)	R	Change in absorbance	Δε (%)	Red-shift (nm)	$K_b \times 10^5$ (M^{-1})	$K_{app} \times 10^5$ (M^{-1})[b]
$[Cu(L)(H_2O)_2](ClO_4)_2$ **1**	235	25	Hypochromism	20	0	0.0013	0.00027
$[Cu(L)(bpy)](ClO_4)$ **2**	272	25	Hypochromism	58	2	0.0360	0.50030
$[Cu(L)(phen)](ClO_4)$ **3**	269	25	Hypochromism	67	4	0.1020	2.24050
$[Cu(L)(dpq)](ClO_4)$ **4**	253	25	Hypochromism	77	5	0.2140	3.18400
$[Cu(L)(dppz)](ClO_4)$ **5**	270	25	Hypochromism	82	9	1.0250	3.90250
$[Cu(L)(dmdppz)](ClO_4)$ **6**	275	25	Hypochromism	61	3	0.0743	1.87302

[a] Measurements were made at R = 25, where R = [DNA]/[Cu complex], concentration of copper(II) complex solutions = 1.0×10^{-5} M.
[b] Concentration of complexes is 0–60 μM; concentration of EthBr is 12.5 μM, concentration of DNA solution is 125 μM.

1–**6**, obviously because the Htdp ligand is expected to be involved in a higher number of hydrogen bonding interactions with DNA.

3.3.2. Fluorescent intercalator displacement (FID) assay

The binding of the complexes to calf thymus DNA has been studied also by fluorescence spectral technique by monitoring the DNA-induced emission intensity of EthBr [74]. The displacement of DNA-bound EthBr by another molecule provides an approximate measure of the affinity of the molecule for dsDNA. Upon adding **1**–**6** (0–60 μM) to CT DNA pretreated with EthBr ([EthBr]/[DNA] = 0.1) in 5 mM Tris–HCl/50 mM NaCl buffer at pH 7.1, the emission intensity of DNA-bound EthBr decreases revealing that all the complexes bind to DNA. To quantify the displacement, the concentration of the complex at which EthBr fluorescence decreases by 50% (assumed to be 50% displacement of EthBr) is calculated. From a plot of the observed intensities against complex concentration the values of apparent DNA binding constant (K_{app}) were calculated using the equation [75],

$$K_{EthBr}[EthBr] = K_{app}[complex]$$

where K_{EthBr} (4.94×10^5 M^{-1}) [66] is the DNA binding constant of EthBr, [EthBr] is the concentration of EthBr (12.5 μM) and [complex] is the concentration of the complex used to obtain 50% reduction in fluorescence intensity of DNA-bound EthBr. The observed decrease in emission intensity of DNA-bound EthBr (Fig. 5) and hence the DNA binding affinities of the complexes follow the order **6**<**5**>**4**>**3**>**2**>**1** (Table 4), which is in conformity with the order of DNA binding affinities obtained from absorption spectral studies (cf. above). Both the electron-transfer from excited EthBr to copper(II) and the EthBr displacement mechanisms would account for the highest value of K_{app} determined for the partially intercalating complex **5**. In contrast, complex **1** is not able to displace EthBr even at higher concentrations. This is consistent with the results obtained by absorption spectral titration (see above), which indicates that the complex **1** does not display any significant intermolecular π–π stacking interaction. The bpy complex **2** shows DNA binding affinity lower than the phen analog, which is consistent with the DNA surface binding of the complex.

3.3.3. Viscosity measurement

Hydrodynamic measurements that are sensitive to changes in length are regarded as the least ambiguous and the most important tests of a DNA binding model in solution, providing reliable evidence for the DNA binding mode [76–78]. The DNA binding modes of the Cu(II) complexes **1**–**6** were investigated by viscosity measurements. The values of relative viscosity (η/η_0), where η and η_0 are the specific viscosities of DNA in the presence and absence of the complexes, were determined and plotted against values of 1/R = 0.0–0.5 (R = [DNA]/[complex]) (Fig. 6). Almost all the copper(II) complexes enhance the viscosity and the ability of the complexes to increase the viscosity of DNA follows the order **6**<**5**>**4**>**3**>**2**>**1**. For **4** and **5**, the viscosity of DNA increases steadily upon increasing the amount of complexes added to CT DNA, which is similar to, but very much lower than that of the classical intercalating compound EthBr. The extended aromatic ring of dppz (**5**) partially intercalated into the DNA base pairs and the higher hydrophobicity of the dppz ring elongate the DNA chain length higher than the dpq complex **4**. The incorporation of two methyl groups on 11,12 positions of dppz ring prevents the partial intercalation of the dppz ring of **6** leading to lengthening the DNA. The complex **1** exerts essentially no effect on DNA viscosity at low binding ratios.

3.4. DNA cleavage studies

The ability of **1**–**6** to cleave DNA was assayed with the aid of gel electrophoresis on supercoiled pUC19 plasmid DNA as the substrate in a medium of 5 mM Tris–HCl/50 mM NaCl buffer (pH 7.1) in the absence of external additives. When circular plasmid DNA is subjected to electrophoresis, the fastest migration will be observed for the supercoiled (SC) form (form I). The SC DNA, if one strand is cleaved, will relax to produce a slower-moving nicked circular (NC) form (form II). If both strands are cleaved, a linear form (LC, form III) will be generated which migrates between form I and form II. Incubation of supercoiled plasmid pUC19 DNA with **1**–**6** for 1 h at 37 °C results in different degrees of cleavage of DNA to NC and LC forms (Fig. 7, Table 5). A peculiar behavior is observed for **5**, which produces an efficient (about 100%) cleavage at low concentrations (40 μM) (Fig. 8). Complex **4** cleaves DNA 90% at 80 μM but lower than complex 5 (Fig. 11). After an analysis of the DNA gel electrophoresis data (Figs. 7–9), the following observations are made. (i) The complex **1** does not participate in nuclease activity (lane 2 in Fig. 7). (ii) The cleavage activity of the complexes follows the same trend as that for DNA binding affinity observed in absorption, emission and viscosity measurements. (iii) Both the complexes **4** and **5** exhibit the highest reactivity in the absence of any additive like ascorbic acid, hydrogen peroxide, etc. (lanes 5 and 6 in Fig. 7). (iv) Most interestingly, the nuclease activity of **5** is found to be proportional to the incubation time (Fig. 9). So the kinetic aspects of the DNA cleavage by **5** have been investigated. Further, (Fig. 8) when the cleavage reactions are carried out under pseudo-Michaelis–Menten conditions by using various concentrations of **5** (10–100 μM) and constant concentration of

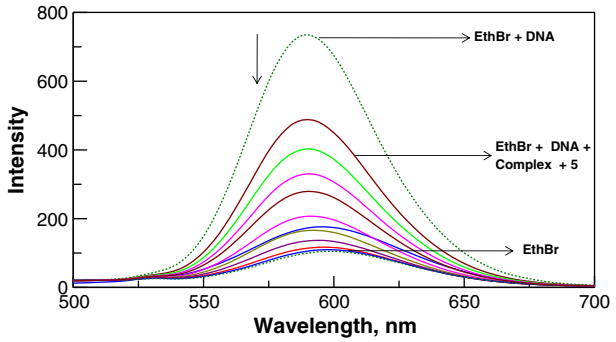

Fig. 5. Emission spectra of EthBr bound to DNA in the absence and presence (continuous lines) of $[Cu(L)(dppz)](ClO_4)$ **5**. The arrow shows the changes in intensity at increasing concentrations of the complex.

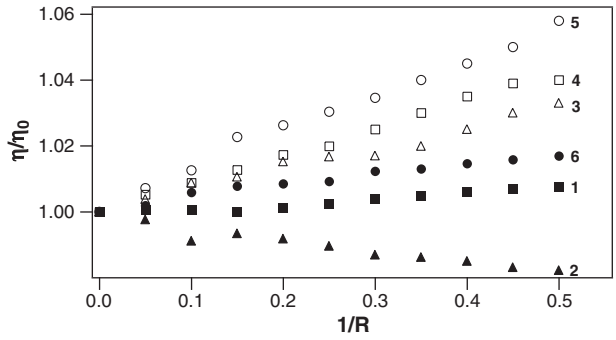

Fig. 6. The effect of complexes **1**–**6** on the viscosity of CT DNA; relative specific viscosity (η/η_0) vs. 1/R = [complex]/[DNA]; [CT DNA] = 500 μM.

DNA (40 μM), the formation of both form II (NC) and form III (LC) from form I are observed (Fig. 8A). The decrease in amount of form I follows pseudo-first-order kinetics and fits well into a single-exponential decay curve (Fig. 8B). Under constant substrate (DNA) concentration and varying catalyst concentration (pseudo Michaelis–Menten conditions), we obtained $V_{max} = 0.0278\ min^{-1}$, $K_M = 32.2\ \mu M$ and $k_{cat} = 6.95 \times 10^{-4}$ (where k_{cat} is defined as V_{max}/[catalyst]) for the double stranded (ds) DNA cleavage. The presence of radical scavengers DMSO, glycerol and methanol does not significantly reduce the efficiency of DNA cleavage (Fig. 10), ruling out the possibility of involvement of diffusible hydroxyl radicals in the cleavage [79]; however, they do not completely rule out the possibility of an oxidative cleavage mechanism. Interestingly, 95% of the cleavage activity is retained when the reactions are performed under rigorously anaerobic conditions, suggesting the non-involvement of activated oxygen species. Thus the mixed ligand complex **5** is one of the few copper(II) complexes that are able to cleave DNA in the absence of a reducing agent under anaerobic conditions [80].

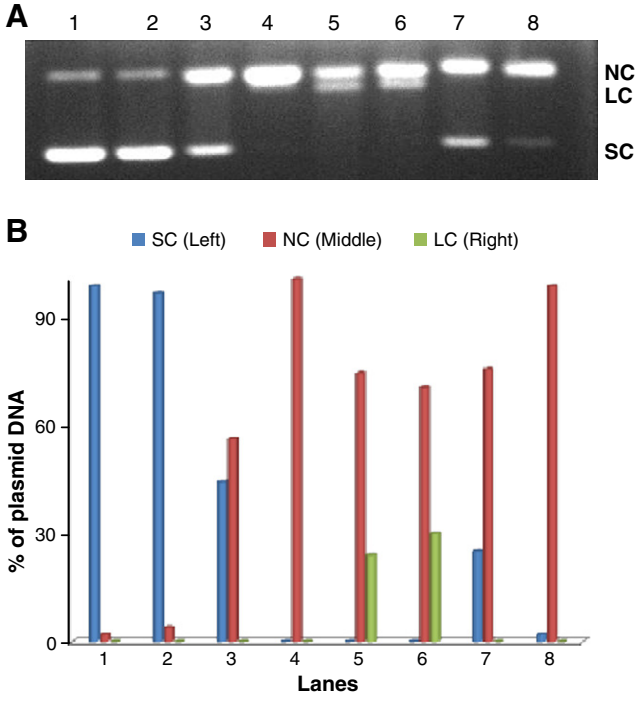

Fig. 7. (A) Gel electrophoresis diagram showing the hydrolytic cleavage of supercoiled pUC19 DNA (40 μM) by complexes **1**–**6** (100 μM) in 5 mM Tris–HCl/50 mM NaCl buffer at pH 7.1 and 37 °C with an incubation time of 1 h: lane 1, DNA; lane 2, DNA + **1**; lane 3, DNA **2**; lane 4, DNA + **3**; lane 5, DNA + **4**; lane 6, DNA + **5**; lane 7, DNA + **6;** lane 8, DNA + $[Cu(dpq)_2(H_2O)]^{2+}$; Forms SC, NC, and LC are supercoiled, nicked circular, and linear circular DNA, respectively. (B) Relative amounts of the different DNA forms in presence of **1**–**6**.

Table 5
Hydrolytic cleavage of super coiled pUC19 DNA (40 μM) by complexes **1**–**6** (100 μM) in the absence of any reducing agent for an incubation time 1 h.

S. No.	Reaction conditions	Form (%)		
		SC	NC	LC
1	DNA control	98	02	00
2	DNA + **1**	96	04	00
3	DNA + **2**	56	44	00
4	DNA + **3**	00	100	00
5	DNA + **4**	00	74	26
6	DNA + **5**	00	70	30
7	DNA + **6**	10	90	00
8	DNA + $[Cu(dpq)_2(H_2O)]^{2+}$	02	98	00

3.5. Anticancer activity studies

3.5.1. MTT assay

Since all the present copper(II) complexes have the ability to strongly bind and cleave DNA in the absence of a reductant, and since DNA cleavage is considered [42,45] as essential for a drug to act as an anticancer agent, the cytotoxicity of the complexes against both human breast cancer cell lines (MCF-7) and human cervical epidermoid carcinoma cell lines (ME 180) were investigated in aqueous buffer solution in comparison with the widely used drug cisplatin under identical conditions by using MTT assay. All the complexes are found to be very active against cancer cells and their IC_{50} values (Table 6) obtained by plotting the cell viability against concentrations of the complexes reveal that all the complexes exhibit cytotoxicity higher than that of cisplatin for both 24 and 48 h incubations. Also, the IC_{50} values at 48 h are lower than those at 24 h clearly indicating that they are dose and time dependent. Further, as revealed by the observed IC_{50} values, the potency of the complexes to kill the cancer cells follows the order **5**>**6**>**4**>**3**>**2**>**1**, revealing that it varies with the mode and extent of interaction of the complexes with

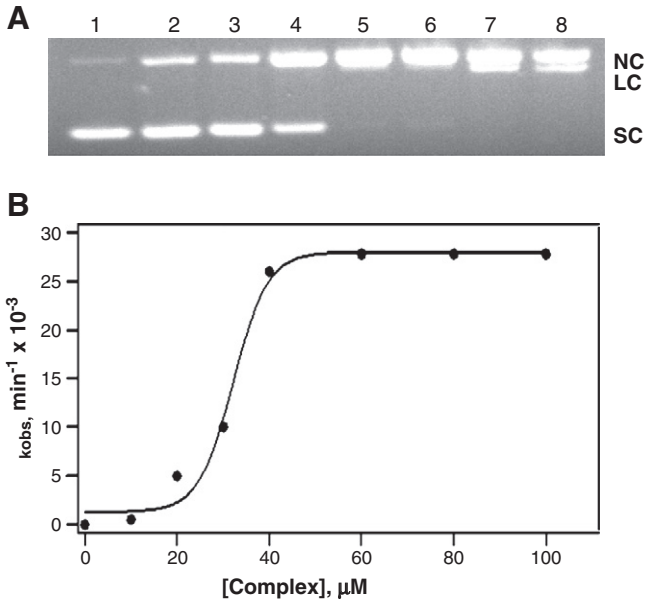

Fig. 8. (A) Gel electrophoresis diagram showing the concentration variation of complex **5** (10–100 μM) in 5 mM Tris–HCl/50 mM NaCl buffer at pH 7.1 and 37 °C with an incubation time of 1 h: lane 1, DNA; lane 2, DNA + **5** (10 μM); lane 3, DNA + **5** (20 μM); lane 4, DNA + **5** (30 μM); lane 5, DNA + **5** (40 μM); lane 6, DNA + **5** (60 μM); lane 7, DNA + **5** (80 μM)**;** lane 8, DNA + **5** (100 μM); Forms SC, NC, and LC are supercoiled, nicked circular, and linear circular DNA, respectively. (B) Plot showing saturation kinetics for the cleavage of plasmid pUC19 DNA (40 μM) with different complex concentrations (10–100 μM) of **5** at 37 °C in 5 mM Tris–HCl/50 mM NaCl buffer at pH 7.1.

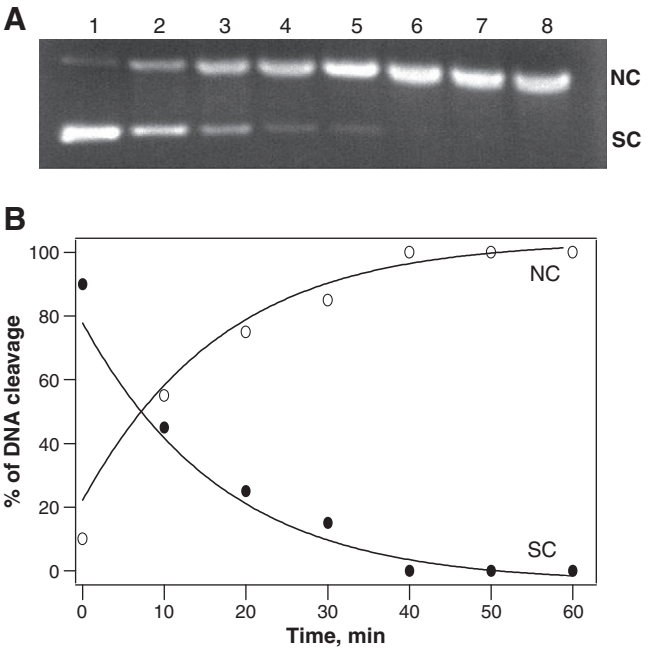

Fig. 9. (A) Time course of supercoiled pUC19 DNA (40 μM) cleavage by complex **5** (40 μM) in a 5 mM Tris–HCl/50 mM NaCl buffer at pH 7.1 and 37 °C with incubation times of 0, 10, 20, 30, 40, 50, and 60 min for lanes 2–8. (B) Hydrolytic cleavage of supercoiled plasmid pUC19 DNA showing the decrease in form I (SC DNA) and the formation of form II (NC DNA) with incubation time using 40 μM concentrations of **5**.

DNA. Interestingly, complexes **5**, **4** and **6** respectively exhibit potency approximately 100, 30 and 50 times more than cisplatin does for both 24 and 48 h incubation. Interestingly, complex **5** shows cell killing activity higher than that of the mixed ligand copper(II) complex of the primary amino acid ligand L-tyr [40], but lower than that of H(tdp), revealing that mixed ligand phenolate complexes enhance the cytotoxicity. Thus, the highest cytotoxicity exhibited by the dppz complex **5** is consistent with the stronger binding of the complex through deeper insertion of the dppz co-ligand in between the base pairs of DNA and its higher ability to cleave DNA in the absence of a reductant is responsible for its potency to induce cell death through different modes.

3.5.2. AO/EB staining assay

The apoptotic morphologies induced by complexes **1**–**6** is investigated by using acridine orange/ethidium bromide (AO/EB) staining and adopting fluorescence microscopy (Fig. 12). The cytological changes observed are classified into four types according to the fluorescence emission and morphological features of chromatin condensation in the AO/EB stained nuclei: (i) viable cells having uniformly green fluorescing nuclei with highly organized structure; (ii) early apoptotic cells (which still have intact membranes but have started undergoing DNA fragmentation) having green fluorescing nuclei, but peri-nuclear chromatin condensation is visible as bright green patches or fragments; (iii) late apoptotic cells having orange to red

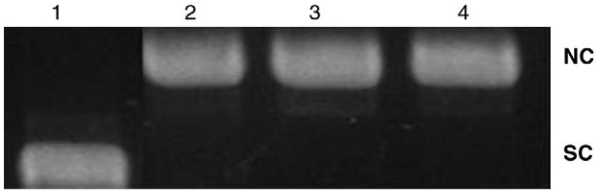

Fig. 10. Gel electrophoresis diagram showing the interaction of **5** (40 μM) with supercoiled pUC19 plasmid DNA (40 μM) in the presence of hydroxyl radical scavengers. Lane 1, DNA (40 μM); lane 2, DNA + **5** (40 μM) + DMSO; lane 3, DNA + **5** (40 μM) + methanol; lane 4, DNA + **5** (40 μM) + glycerol. [See Fig. 8A, lane 5 for control: DNA + 5 alone (40 μM)].

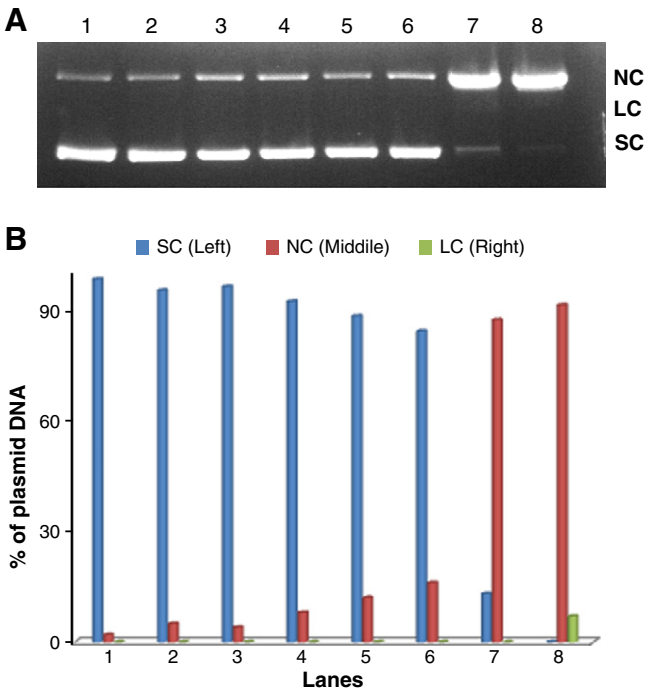

Fig. 11. (A) Gel electrophoresis diagram showing the concentration variation of complex **4** (10–100 μM) in 5 mM Tris–HCl/50 mM NaCl buffer at pH 7.1 and 37 °C with an incubation time of 1 h: lane 1, DNA; lane 2, DNA + **4** (10 μM); lane 3, DNA + **4** (20 μM); lane 4, DNA + **4** (30 μM); lane 5, DNA + **4** (40 μM); lane 6, DNA + **4** (60 μM); lane 7, DNA + **4** (80 μM); lane 8, DNA + **4** (100 μM); Forms SC, NC, and LC are supercoiled, nicked circular, and linear circular DNA, respectively. (B) Relative amounts of the different DNA forms.

fluorescing nuclei with condensed or fragmented chromatin; and (iv) necrotic cells, swollen to large sizes, having uniformly orange to red fluorescing nuclei with no indication of chromatin fragmentation. The morphological changes observed for **5** and **6** suggest that the cells are committed to apoptotic cell death more efficiently compared to other complexes. The positively charged metal complexes adhere to the plasma membrane by electrostatic attraction before its transport across the membrane by the difference in concentration gradient of the complexes [39,40,81], and are eventually released at various organelles in the cell to perform the cellular activities and then interfere with the cellular function of DNA leading to apoptosis. Similar observations have been made by us earlier for the mixed ligand complexes, $[Cu(tdp)(tmp)]^+$ [39], $[Cu(L\text{-}tyr)(5,6\text{-}dmp)]^+$ [40] and $[Cu_2(LH)_2(5,6\text{-}dmp)_2\text{-}(ClO_4)_2]^{2+}$ [81]. Also, **5** causes more cells to preferentially take to one particular mode of cell death during 48 h treatment, and the higher apoptosis-inducing ability may originate from the extended planar surface and hydrophobicity of dppz ligand, which facilitates the permeability of the complex across the cell

Table 6
In vitro cytotoxicity assays for complexes **1**–**6** against MCF-7 breast cancer cell line and human cervical epidermoid carcinoma cell line (ME180) IC_{50} values are in μM.

Complex	IC_{50}, μM[a]			
	MCF-7		ME180	
	24 h	48 h	24 h	48 h
$[Cu(L)(H_2O)_2](ClO_4)$ **1**	40.4 ± 0.10	28.5 ± 0.5	42.0 ± 0.1	30.0 ± 0.2
$[Cu(L)(bpy)](ClO_4)$ **2**	20.0 ± 0.10	15.0 ± 0.2	38.0 ± 0.2	31.0 ± 0.3
$[Cu(L)(phen)](ClO_4)$ **3**	2.00 ± 0.05	1.20 ± 0.10	28.6 ± 0.2	24.6 ± 0.1
$[Cu(L)(dpq)](ClO_4)$ **4**	1.58 ± 0.01	1.55 ± 0.50	19.5 ± 0.1	16.4 ± 0.7
$[Cu(L)(dppz)](ClO_4)$ **5**	0.46 ± 0.02	0.36 ± 0.02	17.0 ± 1.5	13.0 ± 1.3
$[Cu(L)(dmdppz)](ClO_4)$ **6**	0.65 ± 0.01	0.60 ± 0.01	17.7 ± 1.0	14.4 ± 1.3
Cisplatin	45.7 ± 1.0	1.89 ± 0.06	46.7 ± 1.0	33.5 ± 1.0

[a] IC_{50} = concentration of drug required to inhibit growth of 50% of the cancer cells (in μM).

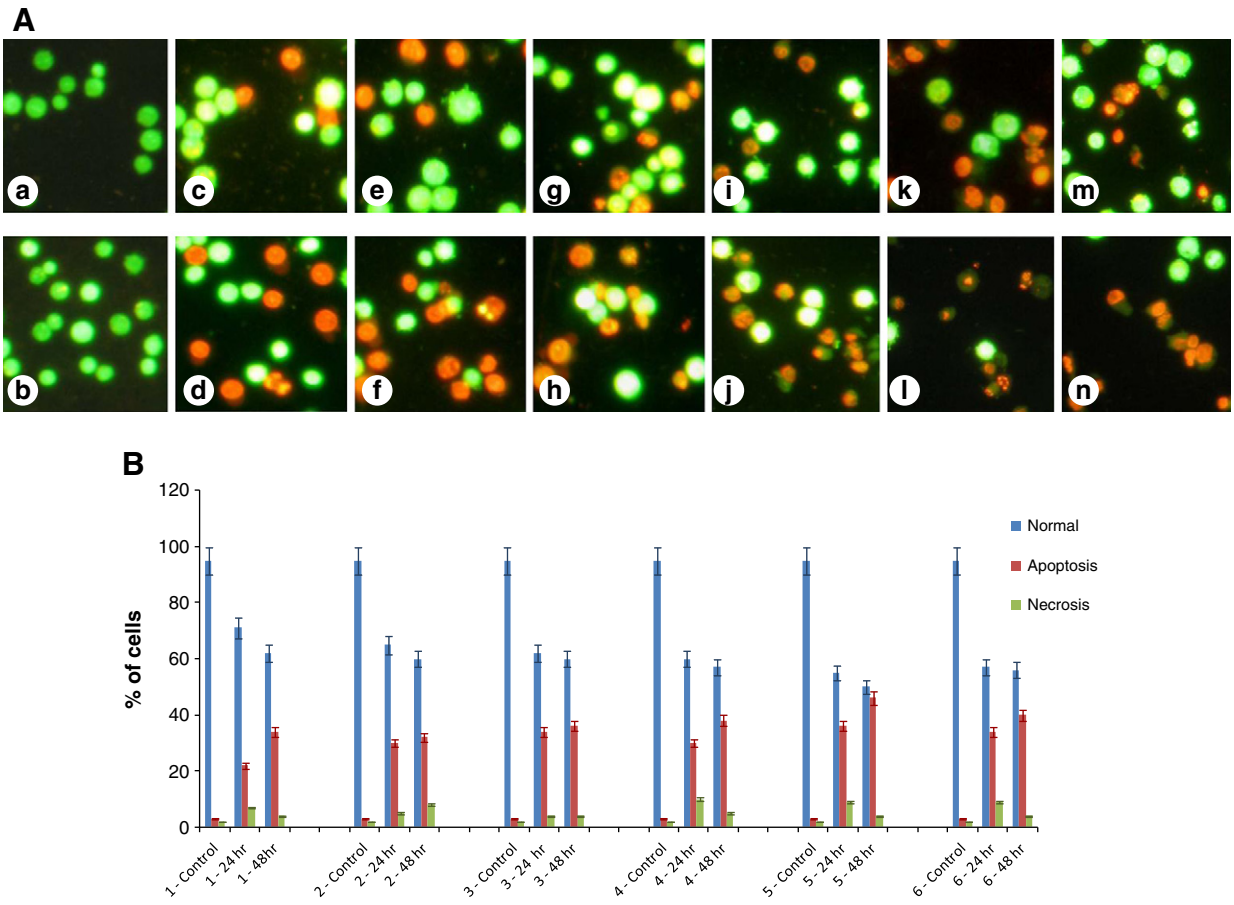

Fig. 12. (A) AO/EB staining of MCF-7 human breast cancer cells. (a, b) Untreated cells, (c, d) treated with complex **1**, (e, f) complex **2**, (g, h) complex **3**, (i, j) complex **4**, (k, l) complex **5** and (m, n) complex **6** with MCF-7 cells at 24 and 48 h of incubations, respectively. (B) Graph shows manual count of apoptotic and necrotic cells in percentage. (Data are mean % ± SD% of each triplicate).

membrane. As the apoptosis-inducing ability is critical in determining the efficacy of an anticancer drug, complexes **5** and **6** with apoptosis-inducing ability higher than that of the other complexes, are more efficacious. Further studies are needed in this direction to confirm the mode of cell death induced by these complexes.

4. Conclusions

Herein we report the isolation of a series of new mixed ligand copper(II) complexes of the type $[Cu(L)(diimine)]^+$, where LH is a tridentate phenolate Schiff base ligand and the results of studying their association with calf thymus DNA by using absorption and emission spectral methods and viscosity technique. The mixed ligand dppz complex exhibits DNA binding affinity higher than that of its analogs, which is due to the higher planarity and hydrophobicity of the dppz co-ligand, and interestingly, it effects more efficient cleavage of double-stranded DNA without the requirement of a reductant. It is noteworthy that the same complex exhibits the highest anticancer activity against human breast cancer cell lines (MCF-7) as well as human cervical epidermoid carcinoma cell lines (ME 180) with its potency higher than that of cisplatin. Thus the mixed ligand copper(II) complex with dppz as co-ligand has the potential to be developed as an anticancer drug for treating human breast cancer and possibly other forms of cancer.

Supplementary data related to this article can be found online at http://dx.doi.org/10.1016/j.jinorgbio.2012.04.018.

Acknowledgments

This work is supported by the Council of Scientific and Industrial Research, New Delhi, India (Grant No. 01(2101)/07/EMR-II). Professor M. Palaniandavar is a recipient of Ramanna National Fellowship of Department of Science and Technology, New Delhi (Grant No. SR/S1/RFIC/01/2007-2010 and SR/S1/RFIC/01/2010–2013). The X-ray diffraction and fluorescence spectral facilities in the Department were created by funding respectively from Department of Science and Technology (DST-FIST), New Delhi and University Grants Commission (SAP), New Delhi.

References

[1] Z. Guo, P.J. Sadler, Angew. Chem. Int. Ed. 38 (1999) 1512–1531.
[2] T. Storr, K.H. Hompson, C. Orvig, Chem. Soc. Rev. 35 (2006) 534–544.
[3] B. Lippert (Ed.), Cisplatin, Chemistry and Biochemistry of a Leading Anticancer Drug, Wiley-VCH, Weinheim, 1999.
[4] J. Reedijk, Chem. Commun. 801–806 (1996).
[5] Z.J. Guo, P.J. Sadler, Adv. Inorg. Chem. 49 (2000) 183–306.
[6] J.D. Roberts, J. Peroutka, N. Farrell, J. Inorg. Biochem. 77 (1999) 51–57.
[7] S.J. Lippard, J.M. Berg, Principles of Bioinorganic Chemistry, University Science Books, Mill Valley, CA, 1994.
[8] R.A. Alderden, D.H. Matthew, W.H. Trevor, J. Chem. Educ. 83 (2006) 724–728.
[9] I. Ott, R. Gust, Arch. Pharm. 340 (2007) 117–126.
[10] I. Meistermann, V. Moreno, M.J. Prieto, E. Molderheim, E. Sletten, S. Khalid, P.M. Rodger, M.J. Hannon, Proc. Natl. Acad. Sci. U. S. A. 99 (2002) 5069–5074.
[11] J.D. Ranford, P.J. Sadler, D.A. Tocher, J. Chem. Soc., Dalton Trans. (1993) 3393–3399.
[12] C.H. Ng, K.C. Kong, S.T. Von, P. Balraj, P. Jensen, E. Thirthagiri, H. Hamada, M. Chikira, Dalton Trans. (2008) 447–454.

[13] A. Hussain, D. Lahiri, M.S. Ameerunisha Begum, S. Saha, R. Majumdar, R.R. Dighe, A.R. Chakravarty, Inorg. Chem. 49 (2010) 4036–4045.
[14] A.C.G. Hotze, S.E. Caspers, D. de Vos, H. Kooijman, A.L. Spek, A. Flamigni, M. Bacac, G. Sava, J.G. Haasnoot, J. Reedijk, J. Biol. Inorg. Chem. 9 (2004) 354–364.
[15] C.G. Hartinger, S. Zorbas-Seifried, M.A. Jakupec, B. Kynast, H. Zorbas, B.K. Keppler, J. Inorg. Biochem. 100 (2006) 891–904.
[16] M.A. Fuertes, C. Alonso, M.J. Perez, Chem. Rev. 103 (2003) 645–662.
[17] M. Cocchietto, G. Sava, Pharmacol. Toxicol. 87 (2000) 193–197.
[18] A. Bergamo, G. Sava, Dalton Trans. (2007) 1267–1272.
[19] M. Magnarin, A. Bergamo, M.E. Carotenuto, S. Zorzet, G. Sava, Anticancer. Res. 20 (2000) 2939–2944.
[20] O.R. Allen, L. Croll, A.L. Gott, R.J. Knox, P.C. McGowan, Organometallics 23 (2004) 288–292.
[21] G. Sava, K. Clerici, I. Capozzi, M. Cocchietto, R. Gagliardi, E. Alessio, G. Mestroni, Anticancer Drugs 10 (1999) 129–138.
[22] B.K. Keppler, M. Henn, U.M. Juhl, M.R. Berger, R. Niebl, F.E. Wagner, Prog. Clin. Biochem. Med. 10 (1989) 41–69.
[23] R.E. Morris, R.E. Aird, P.D. Murdoch, H.M. Chen, J. Cummings, N.D. Hughes, S. Parsons, A. Parkin, G. Boyd, D.I. Jodrell, P.J. Sadler, J. Med. Chem. 44 (2001) 3616–3621.
[24] C. Fernandes, G.L. Parrilha, J.A. Lessa, L.J.M. Santiago, M.M. Kanashiro, F.S. Boniolo, A.J. Bortoluzzi, N.V. Vugman, M.H. Herbst, A. Horn Jr., Inorg. Chim. Acta 359 (2006) 3167–3176.
[25] B.C. Bales, T. Kodama, Y.N. Weledji, M. Pitie, B. Meunier, M.M. Greenberg, Nucleic Acids Res. 33 (2005) 5371–5379.
[26] W.H. Ang, P.J. Dyson, Eur. J. Inorg. Chem. 20 (2006) 4003–4018.
[27] S. Zorzet, A. Sorc, C. Casarsa, M. Cocchietto, G. Sava, Met.-Based Drugs 8 (2001) 1–7.
[28] R. Gagliardi, G. Sava, S. Pacor, G. Mestroni, E. Alessio, Clin. Exp. Metastasis 12 (1994) 93–100.
[29] B.C. Losantos, E. Reisner, C.R. Kowol, A. Roller, S. Shova, V.B. Arion, B.K. Keppler, Inorg. Chem. 47 (2008) 6513–6523.
[30] J.M. Rademaker-Lakhai, D. Van den Bongard, D. Pluim, J.H. Beijnen, J.H. Schellens, Clin. Cancer Res. 10 (2004) 3717–3727.
[31] P.M. May, D.R. Williams, in: H. Sigel (Ed.), Metal Ions in Biological Systems, 12, Marcel Dekker, New York, 1981, (Chapter 7).
[32] H. Sigel (Ed.), Metal Ions in Biological Systems, 13, Marcel Dekker, New York, 1981.
[33] T. Miura, A. Hori-i, H. Mototani, H. Takeuchi, Biochemistry 38 (1999) 11560–11569.
[34] J.A. Crim, H.G. Petering, Cancer Res. 27 (1967) 1278–1285.
[35] S. Roy, P. Uma Maheswari, M. Lutz, A.L. Spek, H. den Dulk, S. Barends, G.P. van Wezel, F. Sek Hartl, J. Reedijk, Dalton Trans. (2009) 10846–10860.
[36] B. Maity, M. Roy, B. Banik, R. Majumdar, R.R. Dighe, A.R. Chakravarty, Organometallics 29 (2010) 3632–3641.
[37] S.T. Von, H.L. Seng, H.B. Lee, S.W. Ng, Y. Kitamura, M. Chikira, C.H. Ng, J. Biol. Inorg. Chem. 17 (2012) 57–69.
[38] S. Zhang, Y. Zhu, C. Tu, H. Wei, Z. Yang, L. Lin, J. Ding, J. Zhang, Z. Guo, J. Inorg. Biochem. 98 (2004) 2099–2106.
[39] V. Rajendiran, R. Karthik, M. Palaniandavar, H.S. Evans, V.S. Periasamay, M.A. Akbarsha, B.S. Srinag, H. Krishnamurthy, Inorg. Chem. 46 (2007) 8208–8221.
[40] S. Ramakrishnan, V. Rajendiran, M. Palaniandavar, V.S. Periasamay, M.A. Akbarsha, B.S. Srinag, H. Krishnamurthy, Inorg. Chem. 48 (2009) 1309–1322.
[41] F. Mancin, P. Scrimin, P. Tecilla, Chem. Commun. 48 (2012) 5545–5559.
[42] L.A. Basile, A.L. Raphael, J.K. Barton, J. Am. Chem. Soc. 109 (1987) 7550–7551.
[43] L. Li, K.D. Karlin, S.E. Rokita, J. Am. Chem. Soc. 127 (2005) 520–521.
[44] S. Ramakrishnan, E. Suresh, A. Riyasdeen, V.S. Periasamy, M.A. Akbarsha, Mallayan Palaniandavar, Dalton Trans. 40 (2011) 3524–3536.
[45] S. Ramakrishnan, E. Suresh, A. Riyasdeen, V.S. Periasamy, M.A. Akbarsha, Mallayan Palaniandavar, Dalton Trans. 40 (2011) 3245–3256.
[46] R. Loganathan, S. Ramakrishnan, E. Suresh, A. Riyasdeen, M.A. Akbarsha, M. Palaniandavar, Inorg. Chem. (in press), http://dx.doi.org/10.1021/ic2017177.
[47] M.G. Pandian, R. Loganathan, S. Ramakrishnan, E. Suresh, A. Riyasdeen, M.A. Akbarsha, M. Palaniandavar, Polyhedron, POLY-D-12-00507 (submitted for publication).
[48] D.S. Sigman, A. Mazumder, D.M. Perrin, Chem. Rev. 93 (1993) 2295–2316.
[49] M.S. Deshpande, A.A. Kumbhar, A.S. Kumbhar, Inorg. Chem. 46 (2007) 5450–5452.
[50] M.O. Connor, A. Kellett, M. McCann, G. Rosair, M. McNamara, O. Howe, B.S. Creaven, S. McClean, A.F. Kia, D. O'Shea, M. Devereux, J. Med. Chem. 55 (2012) 1957–1968.
[51] P.U. Maheswari, S. Roy, H.D. Dulk, S. Barends, G.V. Wezel, B. Kozlevcar, P. Gamez, J. Reedijk, J. Am. Chem. Soc. 128 (2006) 710–711.
[52] J.D. Ranford, P.J. Sadler, D.A. Tocher, Dalton Trans. (1993) 3393–3399.
[53] M.C.B. Oliveira, D. Mazera, M. Scarpellini, P.C. Severino, A. Neves, H. Terenzi, Inorg. Chem. 48 (2009) 2711–2713.
[54] G. Gomori, Proc. Soc. Exp. Biol. Med. 62 (1946) 33–34.
[55] M.E. Reichmann, S.A. Rice, C.A. Thomas, P. Poty, J. Am. Chem. Soc. 76 (1954) 3047–3053.
[56] J.G. Collins, A.D. Sleeman, J.R. Aldrich, I. Greguric, T.W. Hambley, Inorg. Chem. 37 (1998) 3133–3141.
[57] C.M. Dupureur, J.K. Barton, Inorg. Chem. 36 (1997) 33–43.
[58] G. Sheldrick, SHELXL-97, University of Göttingen, Germany, 1999.
[59] SMART & SAINT Software Reference Manuals, v. 5.0, Bruker AXS Inc., Madison, WI, 1998; G. M. Sheldrick, SADABS, Program for area detector adsorption correction, Institute for Inorganic Chemistry, University of Göttingen, Germany, 1996; SHELXTL Reference Manual, v. 5.1, Bruker AXS Inc., Madison, WI, 1998. 32. R. R. Jacobson, Z. Tyeklar, A. Farooq, K. D. Karlin, S. Liu, J. Zubieta, J. Am. Chem. Soc. 110 (1988) 3690–3692.
[60] N.W. Aboelella, S.V. Kryatov, B.F. Gherman, W.W. Brennessel, V.G. Young Jr., R. Sarangi, E.V. Rybak-Akimova, K.O. Hodgson, B. Hedman, E.I. Solomon, C.J. Cramer, W.B. Tolman, J. Am. Chem. Soc. 126 (2004) 16896–16911.
[61] J. Marmur, J. Mol. Biol. 3 (1961) 208–218.
[62] S. Ramakrishnan, M. Palaniandavar, Dalton Trans. (2008) 3866–3878.
[63] B. Mestre, A. Jakobs, G. Pratviel, B. Meunier, Biochemistry 28 (1996) 9140–9149.
[64] M. Blagosklonny, W.S. El-Diery, Int. J. Cancer 67 (1996) 386–392.
[65] A.W. Addison, T.N. Rao, J. Reedijk, J. Van Rijn, G.C. Verschoor, J. Chem. Soc., Dalton Trans. (1984) 1349–1356.
[66] Y. Nishida, K. Takahashi, J. Chem. Soc., Dalton Trans. (1988) 691–699.
[67] M. Palaniandavar, T. Pandiyan, M. Lakshminarayanan, H. Manohar, J. Chem. Soc., Dalton Trans. (1995) 455–461.
[68] M. Velusamy, R. Mayilmurugan, M. Palaniandavar, Inorg. Chem. 43 (2004) 6284–6293.
[69] V. Rajendiran, M. Murali, E. Suresh, M. Palaniandavar, V.S. Periasamy, M.A. Akbarsha, Dalton Trans. (2008) 2157–2170.
[70] A.G. Quiroga, J.M. Perez, I. Lopez-Solera, E.I. Montero, J.R. Masaguer, C. Alonso, C. Navarro-Raninger, J. Inorg. Biochem. 69 (1998) 275–281.
[71] V.A. Bloomfield, D.M. Crothers, I. Tinocco Jr., Physical Chemistry of Nucleic Acids, Harper & Row, New York, 1974, p. 432.
[72] D.L. Boger, S.R. Fink, S.R. Brunette, W.C. Tse, M.P. Hedrick, J. Am. Chem. Soc. 123 (2001) 5878–5891.
[73] V. Rajendiran, M. Murali, E. Suresh, S. Sinha, K. Somasundaram, M. Palaniandavar, Dalton Trans. (2008) 148–163.
[74] J. Liu, T. Zhang, L. Qu, H. Zhou, Q. Zhang, J. Liangian, J. Inorg. Biochem. 91 (2002) 269–276.
[75] B.C. Baguley, M. LeBret, Biochemistry 23 (1984) 937–943.
[76] W.K. Pogozelski, T.J. McNeese, T.D. Tulius, J. Am. Chem. Soc. 117 (1995) 6428–6433.
[77] M. Pitie, B. Meunier, Bioconjug. Chem. 9 (1998) 604–611.
[78] J. Bernadou, G. Pratviel, F. Bennis, M. Girardet, B. Meunier, Biochemistry 28 (1989) 7268–7275.
[79] Q. Liang, D.C. Arianias, E.C. Long, J. Am. Chem. Soc. 120 (1998) 248–252.
[80] E. Lamour, S. Routier, J.L. Bernier, J.P. Catteau, C. Bailly, H. Vezin, J. Am. Chem. Soc. 121 (1999) 1862–1869.
[81] S. Ramakrishnan, D. Shakthipriya, E. Suresh, V.S. Periasamy, M.A. Akbarsha, Mallayan Palaniandavar, Inorg. Chem. 50 (2011) 6458–6471.